Journal of Water Process Engineering 25 (2018) 96–104

Contents lists available at ScienceDirect

Journal of Water Process Engineering

journal homepage: www.elsevier.com/locate/jwpe

A hierarchical porous adsorbent of nano-α-Fe_2O_3/Fe_3O_4 on bamboo biochar (HPA-Fe/C-B) for the removal of phosphate from water

Zongqiang Zhu[a,b,c], C.P. Huang[b,*], Yinian Zhu[a,c,**], Wenhui Wei[a], Hui Qin[a]

[a] College of Environmental Science and Engineering, Guilin University of Technology, Guilin, Guangxi 541004, PR China
[b] Department of Civil and Environmental Engineering, University of Delaware, Newark, DE 19716, USA
[c] Collaborative Innovation Center for Water Pollution Control and Water Safety in Karst Area, Guilin University of Technology, Guilin, Guangxi 541004, PR China

ARTICLE INFO

Keywords:
Bamboo biochar
Hierarchical porous structure
Adsorption
Phosphorus
Nano-iron oxides

ABSTRACT

A novel and magnetic hierarchical porous adsorbent functionalized by coating α-Fe_2O_3/Fe_3O_4 on bamboo biochar (HPA-Fe/C-B) is prepared and tested for the removal of phosphorus from aqueous solutions. The effect of phosphorus (P) concentration, temperature, pH, adsorbent grain size, adsorbent dosage, and contact time on phosphorus adsorption is investigated. Results show that by increasing the initial concentration from 2 to 10 mg-P/L, the phosphorus adsorption capacity of HPA-Fe/C-B (d_g 0.11 mm and contact time 12 h) increases from 0.20 to 2.46, 2.64, and 2.81 mg-P/g and the phosphorus removal is reduced from 99.2 to 49.2 wt%, 99.4–52.8 wt% and 98.8–55.4 wt%, at temperature of 25, 35, and 45 °C, respectively. The phosphorus adsorption capacity of the unpulverized HPA-Fe/C-B (d_g 1.59 mm) is from 0.18 to 0.66 mg-P/g in the concentration range of 2–10 mg-P/L, respectively, which is in the same order of magnitude as that of pulverized HPA-Fe/C-B or nano-size iron adsorbents reported in the literature. Kinetic and equilibrium adsorption results fitted well by the intra-particle diffusion and the Langmuir adsorption isotherm, respectively.

1. Introduction

Phosphorus is an essential primary macronutrient in the water environment. Soluble phosphor in water exists mainly in three forms, i.e., ortho-, poly-, and organic phosphate. Ortho-phosphate includes mainly H_3PO_4, $H_2PO_4^{2-}$, HPO_4^{-} and PO_4^{3-}, which is responsible for stimulating the growth of aquatic macro and microorganisms and leads to eutrophication [1,2]. The phosphate could be easily adsorbed by many plants including algae, and react with specific chemicals such as ferric, lime and alum salts commonly used in wastewater treatment systems [3]. The phosphate concentration in municipal sewage is in the range of 4–15 mg-P/L and exceeds 10 mg-P/L in industrial wastewaters [4]. Therefore, it is necessary to reduce phosphate in wastewater prior to discharge to natural water bodies. Chemical precipitation and biological wastewater treatment are the two traditional phosphorus removal practices, but problems such as costs and availability of carbon source remain.

Adsorption is one of the most widely accepted method for phosphorus removal from dilute aqueous solutions due to high efficiency, low cost, simple operation, and flexibility in application [4–6]. Since the early publication on phosphate adsorption onto hydrous solids by Huang [7], there have been many studies on the synthesis and testing of different adsorbents for phosphate removal. Loganathan et al. have conducted a comprehensive review on phosphate removal from water/wastewater by different methods including adsorption [8]. Most of the adsorbents studied are classified into ones with or without hematite and those single or multiple multivalent valent metal oxides/hydroxides composites [9–12].

In recent years, iron oxides such as Fe_2O_3, Fe_3O_4, FeOOH, and granular ferric hydroxide (GFH) have been applied intensively to environmental pollution remediation. The magnetic property of material such as Fe_3O_4 enables the separation of sorbent by magnet [13,14]. However, the separation of such nanomaterials from solution after water treatment is difficult and extremely expensive. Magnetic separation of nanoparticle size < 15 nm might be ineffective in that the residual nanoparticles in the effluent might impose ecotoxicity on the receiving water [3,14,15]. Hence, much effort has been made to seek best-performing adsorbents for the removal of phosphorus from wastewater.

The presence of pit membranes in the hierarchical porous structure

* Corresponding author.
** Corresponding author at: College of Environmental Science and Engineering, Guilin University of Technology, Guilin, Guangxi 541004, PR China.
E-mail addresses: zhuzongqiang@glut.edu.cn (Z. Zhu), Huang@udel.edu (C.P. Huang), zhuyinian@163.com (Y. Zhu), js3225138@126.com (W. Wei), 495898246@qq.com (H. Qin).

https://doi.org/10.1016/j.jwpe.2018.05.010
Received 30 January 2018; Received in revised form 27 April 2018; Accepted 16 May 2018
Available online 21 July 2018

of bamboo wood increases the three-dimensional network connectivity substantially. Pre-treatment by immersion in boiled agent can improve post-impregnation performance and network connectivity of bamboo biochar. In the present work, A novel adsorbent with magnetic hierarchical porous structure functionalized by coating α-Fe_2O_3/Fe_3O_4 onto bamboo biochar (HPA-Fe/C-B) is synthesized and applied to phosphorus removal from water. Factors, such as contact time, initial phosphorus concentration, solution pH, temperature, and dosage and grain size of HPA-Fe/C-B that may affect phosphate removal are studied. The kinetics and equilibrium adsorption are characterized.

2. Materials and methods

2.1. Preparation and characterization

2.1.1. Adsorbent preparation

Dried bamboo wood (*Phyllostachys pubescens*) are collected and cut into rectangular shape with an average size of *ca.* 30 mm × 10 mm × 3 mm. HPA-Fe/C-B was synthesized according to the following steps. (1) *Boiling in dilute ammonia solution*. Dilute ammonia (5%) solution is used to pre-treat cubical bamboo wood blocks that contains original gums and fats, tropolones and fatty acid amid micropores in boiling process. The wood chips sample are heated in dilute ammonia solution for 6 h as to increase the connectedness between pores and cellular substances [13]. The treated bamboo chips are washed in dionized-distilled water three times and dried at 80 °C in an oven for 1 day. (2) *Impregnation with ferric solution*. Bamboo wood chips after boiling in ammonia solution are subject to precursor treatment at 60 °C in covered beakers. The precursor solution (1.2 mol/L) is made of ferric nitrate as solute and a mixture of ethanol and ultrapure water (1:1) as solvent. Some ethanol solution is added to keep all samples immersed in the precursor solution completely. After 3 d of impregnation, the treated samples are dried in an oven at 80 °C for 1 day. This impregnation–drying operation is repeated three times. (3) *Calcination*. The treated samples after impregnation-drying process are placed in a ceramic crucible and heated slowly from 25 to 600 °C at a rate of ca. 4 °C/min in muffle device (N 11/H/B150, Nabertherm). After continuing heating at 600 °C for 3 h, the HPA-Fe/C-B is obtained when all the samples are cool to room temperature in the muffle.

2.1.2. Surface characterization

The chemical composition, including C, H, N, S, O and Fe, wt%) of HPA-Fe/C-B is determined by CHNOS Elemental Analysis (EA 2400 II, PE,USA) and electronic ultramicrobalance (XP6, Mettler Toledo, Switzerland), The specific surface area of HPA-Fe/C-B is determined by N_2 sorption/desorption using Quantachrome NOVAe1000 and calculated according to the Brunauer- Emmet-Teller (BET) equation. The zeta potential is measured by Zeta Potential Analyzer (Zetasizer Nano ZS90, Malvern, England) with micro-electrophoresis method. HNO_3 and NaOH are used to adjusted the pH value (1.0, 2.0, 3.0, 4.0, 5.0, 6.0, 7.0, 8.0, and 9.0) of a solution containing 0.2 g/L of solid and 10^{-3}M NaCl as supporting electrolyte. The pH_{PZC} is taken at the point of pH where the zeta potential is zero. HPA-Fe/C-B adsorbent before and after phosphorus adsorption are characterized by X-ray diffraction (XRD), Fourier Transfer infrared spectroscopy a (FT-IR), field emission scanning electron microscope(FE-SEM), and energy dispersive x-ray spectroscopy (EDS). The XRD analysis is carried out with a X'Pert PRO X diffractometer using copper K_α radiation at 40 kV and 40 mA. Phase identification of the HPA-Fe/C-B is identified based on hematite (α-Fe_2O_3, reference code 00-005-0637), magnetite (Fe_3O_4, reference code 01-089-0688) and carbon (graphite, reference code 00-001-0646). FT-IR spectra are obtained in KBr pellets with a Thermo Nicolet Nexus 470 Fourier transform spectrometer over wavenumber of 4000–400 cm^{-1}. The structural feature and chemical composition of HPA-Fe/C-B before and after phosphorus adsorption are observed and assessed using FE-SEM and EDS (JEM-6380LV, JEOL, Japan), respectively.

2.2. Batch sorption experiments

2.2.1. Experiments on parameters affecting phosphorus adsorption

The batch phosphorus adsorption experiments are conducted as follows: A given amount of HPA-Fe/C-B adsorbent is weighted and dispersed in a series of 100-mL plastic centrifuge tubes containing 50 mL of phosphate solution at concentration of 2–50 mg-P/L. All suspension samples are shaken (25, 35 or 45 °C) to reach adsorption equilibrium at a speed of 150 strokes per min for two days. After centrifugation at a speed of 4000 rpm for 5 min and filtration with 0.22-μm micro-pore membrane, the filtrate is collected and residual phosphorus concentration measured by the molybdenum blue method using a Lambda 25 UV/VIS spectrophotometer at a detecting wavelength of 700 nm.

The effect of pH (1.0, 2.0, 3.0, 4.0, 5.0, 6.0, 7.0, 8.0, 9.0, and 10.0) on phosphate adsorption is studied at initial phosphate concentration of 2, 5, and 10 mg-P/L at 25 °C. To study the effect of initial phosphate concentration on adsorption, 9 solutions containing initial phosphate concentrations of 2, 5, 10, 15, 20, 25, 30, 40, and 50 mg-P/L are prepared in the presence of 10 g/L HPA-Fe/C-B at pH 3 and 25 °C.

The magnetization intensity of HPA-Fe/C-B was measured as a function of magnetic field strength by using Vibrating Sample Magnetometer (VersaLab, Quantum Design, USA). Results show marked magnetic characteristics of the adsorbent (Fig. S6). Note that 10 g/L of adsorbent only occupied < 10% of the total reactor volume (Fig. S7). After 5 min of magnetic separation operation, the adsorbent material was effectively separated (Fig. S7).

Experiment on the effect of adsorbent dosage is conducted with adsorbent dosage from 0.1 to 1.0 g/50 mL (or 2–10 g/L) in 10 increments of 0.1 g/50 mL (or 2 g/L) and constant phosphorus concentration of 5 mg/L at 25 °C. Experiment to study the effect of grain size is carried out in five adsorbent samples, namely, unpulverized chip (1.59 mm), pulverized powder with different size of 0.58, 0.33, 0.21, 0.16, and 0.11 mm, at 25 °C and initial phosphate concentration of 2, 5, and 10 mg-P/L, respectively.

2.2.2. Kinetics phosphorus adsorption experiments

The adsorption kinetics is studied with a series of 100-mL plastic centrifuge tubes containing 0.5 g of HPA-Fe/C-B in 50 mL of phosphorus solution at initial concentration of 2, 5, and 10 mg-P/L, individually and constant pH 3. The centrifuge tubes are vigorously mixed at speed of 150 rpm. At different time intervals (5, 10, 15, 20, 30, 60, 120, 180, 240, 300, 360, 420, 480, 540, 720, 1080, 1440 and 2880 min), samples are taken and filtered and the filtrates are collected for the analysis of residual phosphorus concentration.

2.2.3. Equilibrium phosphorus adsorption experiments

A series of phosphorus solutions containing initial concentration of 2, 5, 10, 15, 20, 25, 30, 40, and 50 mg-P/L) are employed for equilibrium adsorption experiments. All solutions contain 10 g/L HPA-Fe/C-B with pH being adjusted to 3. All solid-solution mixtures are mixed over a shaker at constant temperature of 25, 35 and 45 °C, respectively. Procedures for the measurement of residual phosphorus concentration follow that of kinetics experiments.

3. Results and discussion

3.1. Characterization

The weight percent of C, H, O, N and S is 25.18–25.85, 1.02–1.49, 25.61–26.08, 0.85–0.99, and 0.18–0.24%, respectively. The Fe content is 45.51–47.02% and the BET surface area is 198.1 m^2/g.

X-ray diffraction (XRD) technique is employed to characterize the crystalline structure of HPA-Fe/C-B adsorbent before and after phosphorus removal experiments. Results show that magnetite, hematite, and carbon are present on the HPA-Fe/C-B surface (Fig. 1).

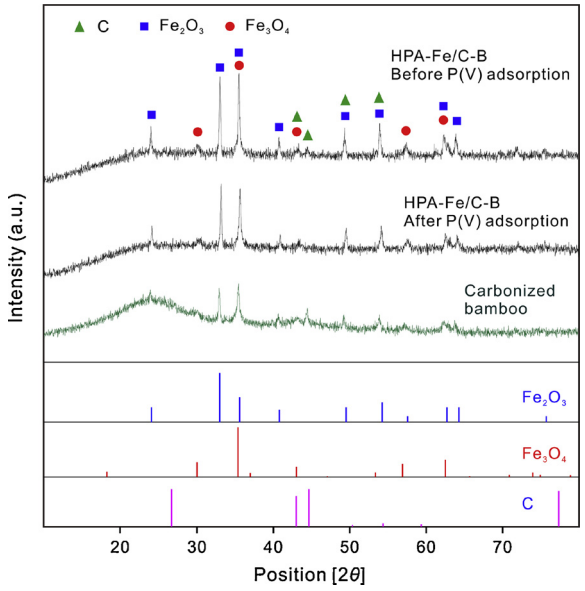

Fig. 1. XRD patterns of the HPA-Fe/C-B before and after phosphorus adsorption. Adsorption experimental conditions: initial phosphorus concentration = 10 mg/L; initial pH = 3.0; adsorbent dose = 10 g/L; geometric mean adsorbent grain size = 0.11 mm.

The location and intensity of XRD peaks match perfectly three reference peaks. The peaks at 2θ of 30.22°, 35.61°, 57.50°, and 62.42° correspond to Fe_3O_4 (magnetite, reference code 01-089-0688), the peaks at 2θ of 24.11°, 33.13°, 35.61°, 40.85°, 49.44°, 54.04°, 62.42°, and 63.98° belong to α-Fe_2O_3 (hematite, reference code 00-005-0637), and the peaks at 2θ of 42.82°, 44.60°, 50.38°, and 54.23° are identified as carbon (graphite, reference code 00-001-0646).

According to Fig. 1, the carbonized bamboo, HPA-Fe/C-B before and after phosphorus adsorption are indistinguishable. Results of quantitative phase analysis of XRD diffraction profile by the Rietveld method show that HPA-Fe/C-B consists of 59.78% Fe_3O_4 and 40.22% α-Fe_2O_3.

Fig. 2 shows the FT-IR pattern of HPA-Fe/C-B before and after phosphorus adsorption, which reveals a Fe–O peak at 469.47 cm^{-1}. After phosphorus adsorption, the PO_4^{3-} peaks due to O–P–O vibration band appear around 869.92, 812.71, and 767.76 cm^{-1}, and due to the P–O stretching are seen around 447.40–474.27 cm^{-1}.

The FE-SEM pattern of HPA-Fe/C-B clearly shows the presence of the original hierarchical porous framework of bamboo wood with three distinct pores: (a) *macropores* formed on the vessels at diameter around 50–75 μm; (b) *mesopores* formed on parenchyma cells at diameter around 10–30 μm and fibres at diameter around 1–15 μm; (c) *micropores* originated from the capillary walls and parenchyma cells that provide plentiful pits at 2.0–289.0 nm (Fig. 3). The total pore volume, 0.12 cm^3/g, is similar to that of biochar prepared from soybeans (0.19 cm^3/g), and larger than biochars produced from corn stalks (0.09 cm^3/g), rice stalks (0.05 cm^3/g), poultry manure (0.09 cm^3/g), cattle manure (0.08 cm^3/g), and pig manure (0.05 cm^3/g), respectively [13].

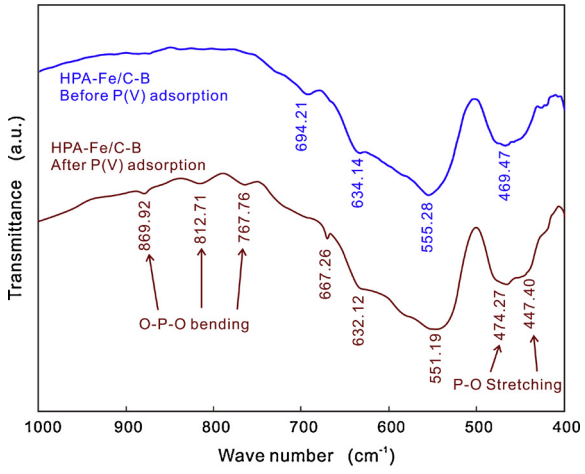

Fig. 2. FT-IR spectra of HPA-Fe/C-B before and after phosphorus adsorption.

The EDS spectrum (Fig. 4) is obtained for the unpulverized HPA-Fe/C-B exposed to high phosphate concentration (100 mg-P/L). The EDS spectrum of HPA-Fe/C-B shows that the characteristic peak of phosphorus appears at 2.01 keV after phosphorus adsorption. The phosphorus adsorption capacity is estimated at 0.82 wt% based on the SEM-EDS peak area ratio. It also confirms that the phosphorus ion (0.82 wt %,) is associated with the HPA-Fe/C-B surface.

3.2. Effect of adsorption variables

3.2.1. Initial phosphorus concentration and temperature

Fig. 5 shows the phosphorus adsorption (a) and the percent removal (b) as a function of equilibrium and initial phosphorus concentration, respectively, at different temperature.

Temperature has an insignificant effect on phosphorus adsorption. With increasing phosphorus concentration (from 2 to 50 mg-P/L), the maximum phosphorus adsorption capacity increases from 0.20 to 2.46, to 2.62, and to 2.81 mg-P/g at 25, 35, and 45 °C, respectively. On the contrary, the percent removal reduces from 99.2 to 49.2, from 99.4 to 52.8, and 98.8–56.2 wt% at 25, 35, and 45 °C, respectively. Results clearly indicate the exothermal nature of phosphorus adsorption onto HPA-Fe/C-B adsorbent.

3.2.2. Solution pH

Fig. 6 shows the effect of final pH on phosphorus adsorption.

The pH has significant effect on phosphorus adsorption, due mostly to the pH-dependent phosphate speciation and the surface charge of the HPA-Fe/C-B [11]. The phosphorus adsorption capacity (and percent removal) increases with increase in pH to a maximum level at pH ~3, then slightly decreases with further increase in pH. The maximum adsorption capacity (and the corresponding percent removal) are 0.20 mg/g (99.21%), 0.49 mg/g (97.50%), and 0.84 mg/g (84.44%) at initial phosphorus concentration of 2.0, 5.0, and 10.0 mg/L, respectively. This pattern is the same as that reported for other adsorbents [16,17].

Dihydrogen phosphate ($H_2PO_4^-$), monohydrogen phosphate (HPO_4^{2-}) and phosphate (PO_4^{3-}) are major inorganic phosphorus species in aqueous solution. Surface charge can affect the adsorption of phosphate species, which again is influenced by solution pH. The pH_{PZC} of HPA-Fe/C-B, bamboo biochar, α-Fe_2O_3, and Fe_3O_4 are 3.1, 2.3, 5.2, and 5.7, respectively. The pH_{pzc} of HPA-Fe/C-B is close to literature data [17]. Fe_3O_4 magnetic nanoparticle prepared via carbodiimide activation has a pH_{PZC} of 6.7 [18–20]. The pH_{PZC} (*ca.* 3.1) of HPA-Fe/C-B is between that of Fe_3O_4 and Fe_2O_3.

At pH < pH_{PZC} (*ca.* 3.1), $H_2PO_4^-$ is the predominant species and HPA-Fe/C-B is positively charged, which favours electrostatic attraction of anions, such as $H_2PO_4^-$. [17,18]. Although it must be mentioned that electrostatic interaction may play a role on ion adsorption, other process such as formation of specific chemical bonds between anions and similarly-charged surface can occur Huang [7] studied phosphate adsorption on γ-Al_2O_3 surface and reported significant adsorption of anionic phosphate ions onto negatively charge hydrous solid surface.

The surface acidity of biochar can be visualized as derived from the protonation/deprotonation equilibrium of surface hydroxy groups, that is, upon hydration, the surface is occupied by OH functional group, which undergoes protonation and deprotonation reaction (Eqs. (1) & (2)) [7,25].

$$\equiv S{-}OH + H^+ = \equiv S{-}OH_2^+;\ 1/K_{a1}^{int} \quad (1)$$

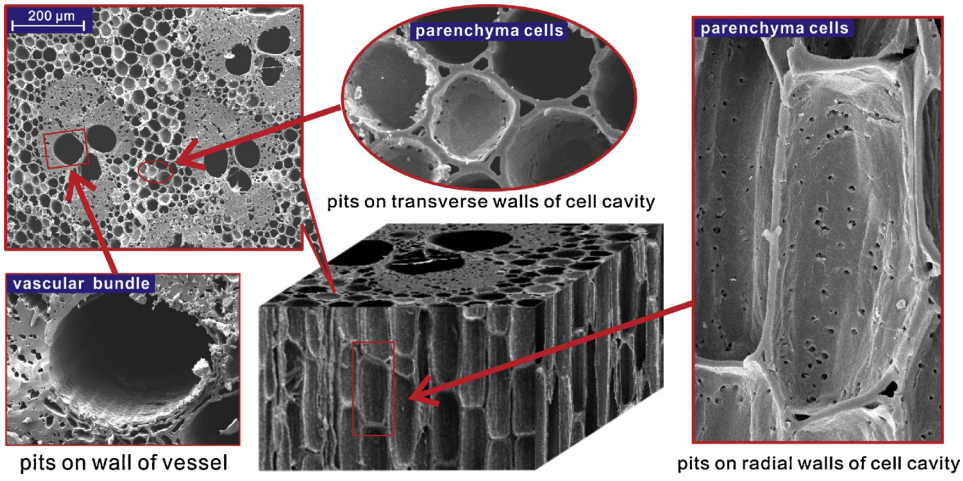

Fig. 3. The FE-SEM image of HPA-Fe/C-B.

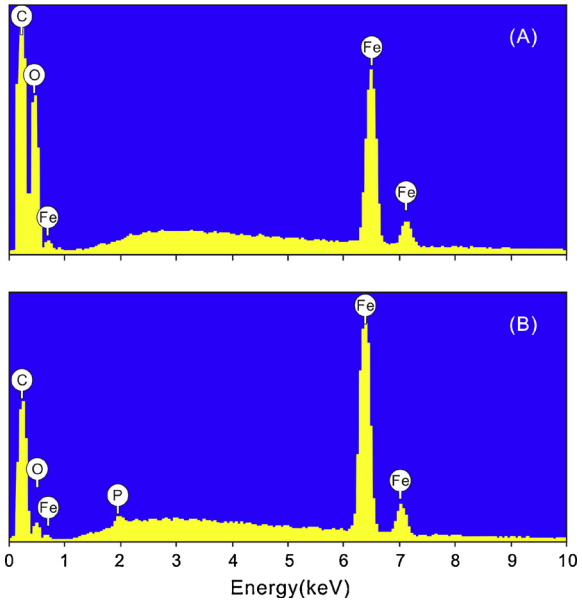

Fig. 4. EDS spectrum of the HPA-Fe/C-B before (a) and after (b) phosphorus adsorption.

$$\equiv S{-}OH = \equiv S{-}O^- + H^+;\ K_{a2}^{int} \quad (2)$$

Where $\equiv S{-}OH_2^+$, $\equiv S{-}OH$, and $\equiv S{-}O^-$ are positively, neutral and negatively charged surface hydroxy species, respectively. K_{a1}^{int} and K_{a2}^{int} are the intrinsic surface acidity constants. Based on zeta potential measurement as a function of pH, it is possible to calculate the acidity constant of HPA-Fe/C-B [7,25]. Result shows that the intrinsic acidity constants are 1.5 and 4.7 for pK_{a1}^{int} and pK_{a2}^{int}, respectively. Thus, at pH < 1.5, the dominant surface functional group of HPA-Fe/C-B is $\equiv S{-}OH_2^+$. At 1.5 < pH < 4.7, $\equiv S{-}OH$ is the dominant hydroxy species of HPA-Fe/C-B. At pH > 4.7, $\equiv S{-}O^-$ dominates the active surface site on HPA-Fe/C-B. In the pH range of significant phosphate adsorption, $H_2PO_4^-$ is the major species; therefore, one can expect the following reactions take place between the biochar surface and the phosphate species (Eqs. (3) & (4)).

$$\equiv S{-}OH_2^+ + H_2PO_4^- = \equiv S{-}PO_4H_2 + H_2O \quad (3)$$

$$\equiv S{-}OH + H_2PO_4^- = \equiv S{-}PO_4H^- + H_2O \quad (4)$$

Significant phosphate adsorption on $\equiv S{-}OH_2^+$ or $\equiv S{-}OH$ site takes place at 1.0 < pH < 3.1 (Eq. (3)) or 1.5 < pH < 4.7 (Eq. (4)),

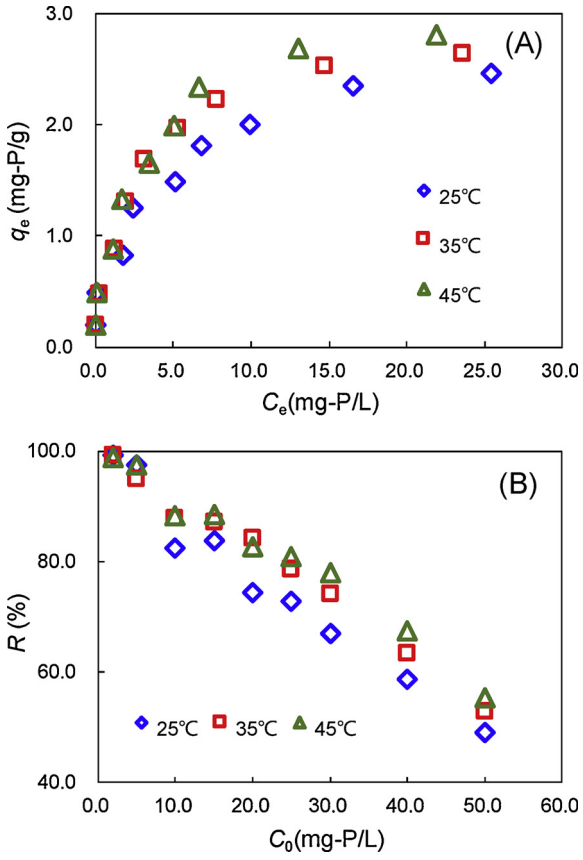

Fig. 5. Effect of initial phosphorus concentration on phosphorus adsorption by HPA-Fe/C-B adsorbent: a) adsorption capacity (q_e), and (b) percent removal (R %). Experimental conditions: initial solution pH = 3; adsorbent dosage = 10 g/L; geometric mean adsorbent grain size = 0.11 mm.

which results in the formation of mono-dentate HPA-Fe/C-B-$H_2PO_4^-$ surface complex. Intuitively, the negatively charged site $\equiv S{-}O^-$ will repel anionic phosphate species at high pH, i.e., 4.7 < pH < 7.0. (Eq. (5)).

$$\equiv S{-}O^- + H_2PO_4^- = \equiv S{-}PO_4^{2-} + H_2O \quad (5)$$

Not run in the present study, nonetheless, the regeneration of phosphate laden HPA-Fe/C-B adsorbent can be readily achieved by acid (pH < ~1.5) or alkaline (pH > ~8.5) stripping as shown in Fig. 7. The durability of the HPA-Fe/C-B adsorbent is not assessed specifically

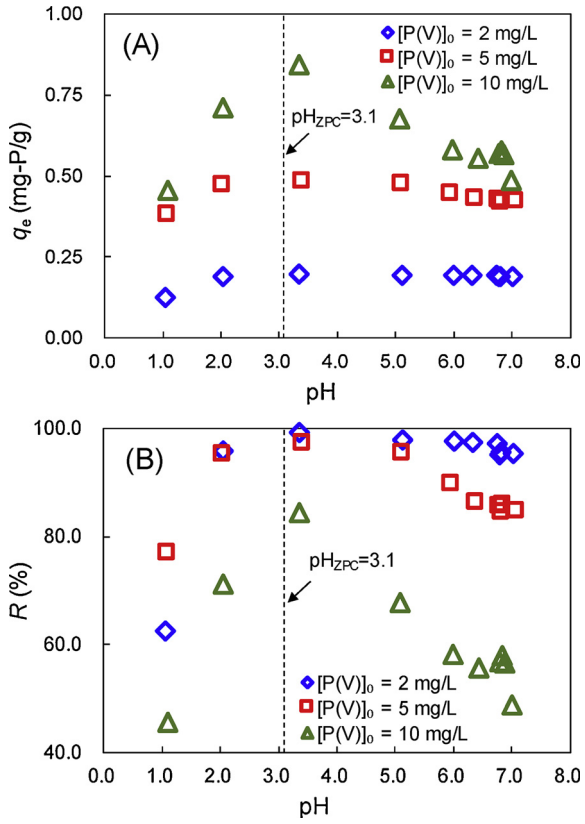

Fig. 6. Effect of solution pH on phosphorus adsorption onto the HPA-Fe/C-B adsorbent: (a) adsorption capacity (q_e), and (b) percent removal (R%). Experimental conditions: initial phosphorus concentration = 2, 5, & 10 mg/L; adsorbent dose = 10 g/L; geometric mean adsorbent grain size = 0.11 mm; temperature = 25 °C.

in the present study. Ultimately, the individual material such as magnetite might be lost in multiple phosphate adsorption cycles at acidic pH. However, hematite nanoparticles are formed at high temperature of 600 °C and might be anodized under acidic condition, which should enhance its stability in lieu of dissolution"

3.2.3. Adsorbent dose

The phosphorus adsorption onto the HPA-Fe/C-B adsorbent is studied by varying adsorbent dose (0.1, 0.2, 0.3, 0.4, 0.5, 0.6, 0.7, 0.8, 0.9 and 1.0 g in 50 mL phosphorus solution or 2, 4, 6, 7, 8, 10, 12, 14, 16, 18, and 20 g/L) and 3 initial phosphorus concentrations (2, 5, and 10 mg-P/L) while keeping constant the initial pH, sorbent grain size, and temperature (Fig. 7).

Results show that the phosphorus adsorption capacity decreases from 0.87 to 0.10 mg-P/g, from 1.66 to 0.25 mg-P/g and from 1.84 to 0.44 mg-P/g, at initial phosphate concentration of 2, 5, and 10 mg-P/L, respectively. The corresponding phosphorus removal percent (average of three independent runs) increases from 86.6 to 99.8 wt%, 66.5–99.9 wt%, and 36.8–88.8 wt% at adsorbent dose of 2, 10, and 20 g/L, respectively. Increase in phosphate adsorption with increase in adsorbent dosage can be attributed to increase in adsorbent surface adsorption site. The phosphorus capacity reaches a plateau at adsorbent dosage of 10 g/L, obviously due to the depletion of phosphate species in the solution [13].

3.2.4. Adsorbent grain size

Six adsorbent grain sizes (1.59, 0.58, 0.33, 0.21, 0.16, and 0.11 mm), three types of adsorbent (carbonized bamboo wood, the saw dust of bamboo wood and α-Fe_2O_3 powder), three initial phosphorus concentrations (2, 5, 10 mg/L) at initial pH 3 and 25 °C are studied.

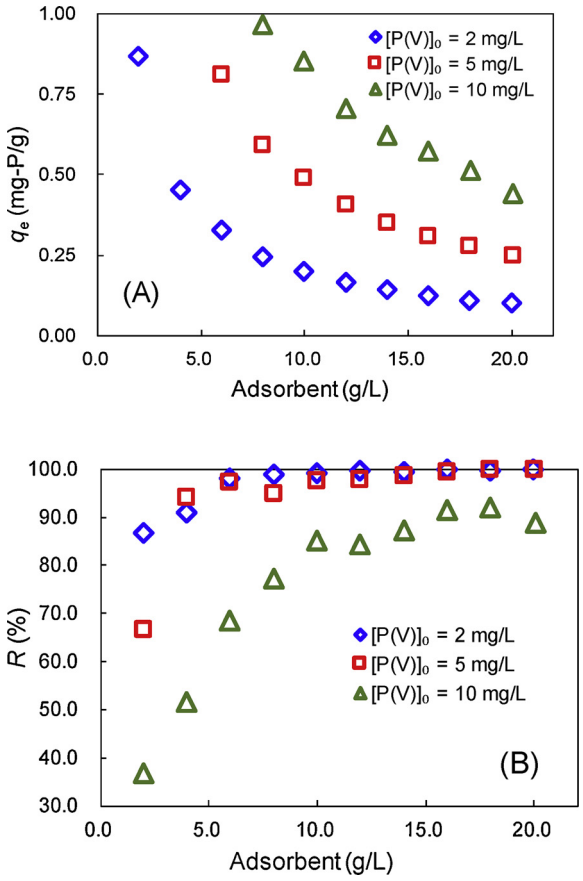

Fig. 7. Effect of adsorption dose on phosphorus adsorption onto the HPA-Fe/C-B adsorbent: (a) adsorption capacity (q_e), and (b) percent removal (R%). Experimental conditions: initial phosphorus concentration = 2, 5, & 10 mg/L; initial pH = 3.0; geometric mean adsorbent grain size = 0.11 mm; temperature = 25 °C.

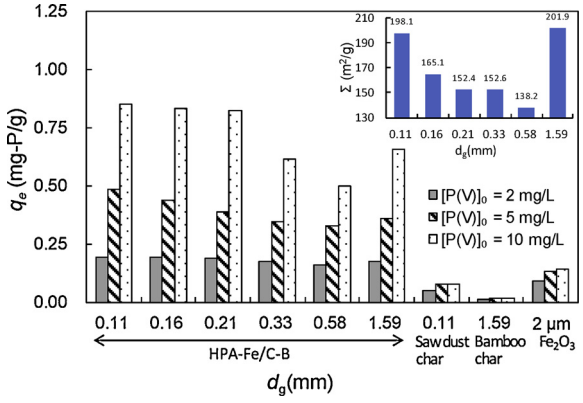

Fig. 8. Effect of adsorbent grain size and type on phosphorus adsorption onto the HPA-Fe/C-B adsorbent. Experimental conditions: initial phosphorus concentration = 2, 5, & 10 mg/L; initial pH = 3.0; adsorbent dose = 10 g/L; temperature = 25 °C. Inset is plot of specific surface area versus mean geometric size.

Fig. 8 summarizes the phosphorus adsorption capacity as a function of grain size.

Generally, the smaller grain size the greater specific surface area, therefore it is possible to increase the adsorption capacity and percent removal by manipulating the grain size. However, smaller particles tend to clump together during adsorption process, which renders it difficult for solid-water separation after application. Obviously,

Table 1
Comparison of phosphate adsorption capacity of HPA-Fe/C-B with other iron oxides.

Adsorbent	pH	Concentr. (mg/L)	BET ASP (m^2/g)	Particle size (mm)	Tem. (K)	Capacity (mg-P/g)	Ref.
PBGC-Fe/C	3	2	59.2	d_g = 1.59	298	0.18	[16]
PBGC-Fe/C	3	5	59.2	d_g = 1.59	298	0.34	[16]
PBGC-Fe/C	3	10	59.2	d_g = 1.59	298	0.69	[16]
PBGC-Fe/C	3	2–10	–	d_g = 0.11	298	1.53	[16]
PBGC-Fe/C	3	2–10	–	d_g = 0.11	308	1.63	[16]
PBGC-Fe/C	3	2–10	–	d_g = 0.11	318	1.81	[16]
Magnetite (natural)	7	0.31–46.46	0.13	< 0.25	room	0.42	[21]
Magnetite (synthetic)	7	0.31–46.46	1.74	< 0.25	room	1.06	[21]
Magnetite (MIO)	4	200	–	1.7 μm	room	2.18	[22]
Hematite (B1)	6	0–8	16	70–130 nm	298	0.62	[23]
Hematite (B2)	6	0–8	17	70–135 nm	298	1.11	[23]
Hematite (B3)	6	0–8	17	70–135 nm	298	0.92	[23]
Hematite (B4)	6	0–8	23	60–200 nm	298	1.13	[23]
Hematite (B5)	6	0–8	20	45–220 nm	298	0.657	[23]
Hematite + Gibbsite	7	1–300	–	0.22 μm	277 ~ 318	0.025 ~ 0.19	[24]
Hematite	3	13.74	47.01	–	298	3.72	[25] [26]
Magnetite nanoparticles	3	15.5	31	–	298	0.5–3.5	[27]
Magnetite microparticles	7	0.5	–	–	room	3.2	[28]
Magnetite microparticles (CMC-MP)	7	0.5	–	4.1 μm	room	1.9	[28]
Hematite	3.39	3–20	9.12	–	room	0.57	[29]
Mg-Fe-Zr-LDYs	4	10	–	–	room	23	[9]
Mg-Al-Zr-LDHs	–	–	100	–	room	35	[10]
Mg-Al-LDH-Fe3O4	–	–	–	–	room	37	[11]
ZrO2-Fe3O4	–	–	–	–	room	16	[12]
HPA-Fe/C-B	3	2	198.1	d_g = 1.59	298	0.18	Present study
HPA-Fe/C-B	3	5	198.1	d_g = 1.59	298	0.36	Present study
HPA-Fe/C-B	3	10	198.1	d_g = 1.59	298	0.66	Present study
HPA-Fe/C-B	3	2–10	–	d_g = 0.11	298	2.85	Present study
HPA-Fe/C-B	3	2–10	–	d_g = 0.11	308	2.89	Present study
HPA-Fe/C-B	3	2–10	–	d_g = 0.11	318	3.08	Present study

adsorbents with large grain size but have high total surface area are ideal for achieving high adsorption efficiency and enhancing application potential.

In our study, pulverizing HPA-Fe/C-B only results in slight increase in BET surface area. The hierarchical porous microstructure of unpulverized HPA-Fe/C-B is composed of macropores (65.1%), mesopores (31.7%), and micropores (3.2%) with pore size in the range of 0.8–87,000 nm. Macropores and mesopores are the major structures of the hierarchical porous microstructure of HPA-Fe/C-B. Further grinding of HPA-Fe/C-B does not increase the specific surface area. Fig. 8 shows that the phosphorus adsorption capacity is related to the specific surface areas but not the grain size, especially at high initial phosphorus concentration (i.e., 5 and 10 mg-P/L). The phosphorus adsorption capacity (and removal percentage) of unpulverized HPA-Fe/C-B (d_g 1.59 mm) are 0.18 mg-P/g (87.9%), 0.36 mg-P/g (71.8%) and 0.66 mg-P/g (66.0%) at initial phosphorus concentration of 2, 5, and 10 mg/L, respectively. For pulverized HPA-Fe/C-B, the smaller grain size the greater the BET specific surface area and thus the greater absorption capacity. For pulverized HPA-Fe/C-B with geometric mean adsorbent grain size of 0.11 mm, the maximum phosphorus adsorption capacity (percent removal) is 0.20 mg-P/g (97.7%), 0.48 mg-P/g (96.9%), 0.85 mg-P/g (85.1%) at the initial phosphorus concentration of 2, 5, and 10 mg-P/L, respectively, which is close to that of unpulverized adsorbents. The result also indicates that the unpulverized HPA-Fe/C-B, with intrinsic hierarchical porous microstructure, has higher phosphorus adsorption capacity and removal percentage than charcoal made of bamboo wood (d_g 0.11 mm), sawdust of bamboo wood (d_g 1.59 mm), and α-Fe_2O_3 powder at selected initial total phosphorus concentrations. Obviously, the unique hierarchical porous microstructure of HPA-Fe/C-B endowed from the intrinsic template of bamboo wood, has vast macropores and mesopores that contribute to fast phosphorus adsorption. Hence, HPA-Fe/C-B can still have favourable phosphorus adsorption capacity without further grinding.

Table 1 lists the phosphorus adsorption capacity of HPA-Fe/C-B and other iron (Fe^{2+}/Fe^{3+}) oxides adsorbents reported in the literature. The result indicates that HPA-Fe/C-B is among the best adsorbent for phosphorus adsorption from aqueous solution.

Zhu.et al. [16] have reported phosphorus adsorption capacity of PBGC–Fe/C at 0.18 and 0.66 mg/g at initial phosphorus concentration of 2 and 10 mg/L, respectively. Barber [21] study the phosphorus adsorption capacity of natural and synthetic magnetite under static conditions. The naturally occurring magnetite (BET ASF = 0.13 m^2/g, particle size < 0.25 mm) is obtained from the Stanford University Research Mineral Collection and the synthetic magnetite (BET ASF = 1.74 m^2/g, particle size < 0.25 mm) is purchased from Aldrich Chemical Company. The phosphorus adsorption capacity of the natural and synthetic magnetite at pH 7 and initial phosphorus concentration of 0.31–46.46 mg/L are 0.42 and 1.06 mg/g, respectively [21]. Choi et al. [22] study phosphorus adsorption by synthetic magnetite (MIO) at pH 4 and the initial phosphorus concentration of 200 mg/L and report adsorption capacity of 2.18 mg/g. Colombo et al. [23] reported phosphate adsorption capacity of hematite in the range of 0.66–1.13 mg/g and attribute the variation in adsorption capacity to crystal size and morphology (specific surface area 16–23 m^2/g, grain size from 70–130 nm to 45–220 nm). Daou et al. [27] and Pan et al. [28] reported phosphorus adsorption capacity of 0.5–3.5 and 3.2 mg/g for nano- and

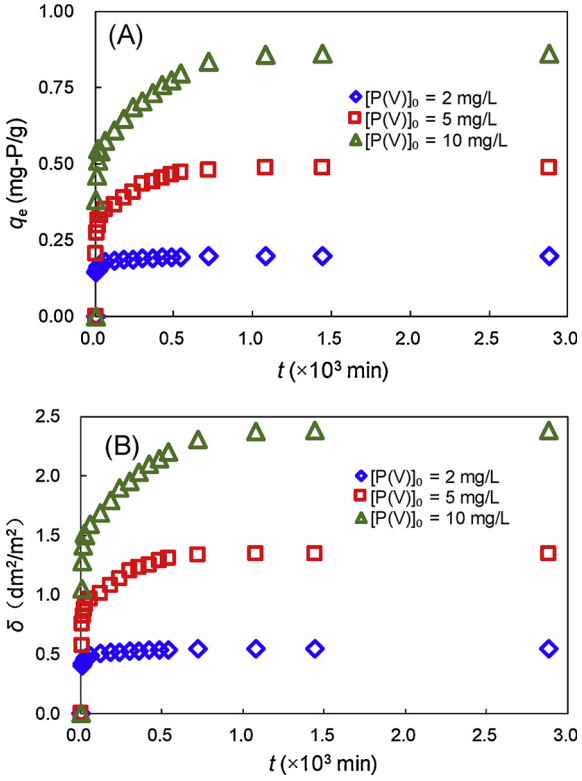

Fig. 9. Effect of contact time on phosphorus adsorption capacity (q_e) and surface coverage (δ) on HPA-Fe/C-B. Experimental conditions: initial phosphorus concentration = 2, 5, & 10 mg/L; initial pH = 3.0; adsorbent dose = 10 g/L; geometric mean adsorbent grain size = 0.11 mm; temperature = 25 °C.

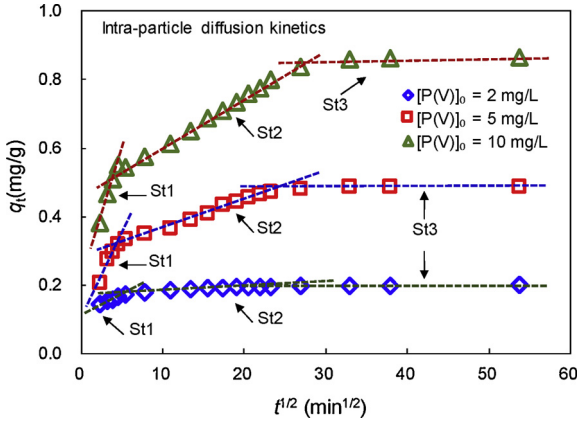

Fig. 10. Intra-particle diffusion kinetics fitting for phosphorus adsorption onto the HPA-Fe/C-B. Where St stands for stage. Experimental conditions: initial phosphorus concentration = 2, 5, & 10 mg/L; initial pH = 3.0; adsorbent dose = 10 g/L; geometric mean adsorbent grain size = 0.11 mm; temperature = 25 °C.

micro-sized magnetite, at pH 3 and pH 7, respectively. Table 1 also shows that the unpulverized HPA-Fe/C-B adsorbent has average phosphorus adsorption capacity similar to those of fine particles or nanoparticles of iron oxides reported in the literature [21–28].

3.3. Adsorption kinetics

Fig. 9 shows the effect of the contact time on phosphate adsorption capacity and surface coverage of HPA-Fe/C-B. The phosphorus adsorption capacity (mg-P/g) and the surface coverage (θ) increase rapidly with contact time until gradually approaching the equilibrium state, which is due to the continuous decease in the driving force, i.e., difference between equilibrium and temporal adsorption density ($q_e - q_t$). The phosphorus adsorption capacity remains almost constant after 1, 12, and 18 h at 25 °C, pH 3, and initial concentration of 2, 5, and 10 mg-P/L, respectively. Phosphorus adsorption takes place rapidly at the onset of adsorption experiment due to adsorption onto macropores and mesoporoes (ionic radius of phosphate ≈ 5.3 Å [29]). Further adsorption onto mesopores and micropores needs more energy and contact time. Result clearly confirms strong and rapid interactions between phosphate and HPA-Fe/C-B, especially at low phosphorus concentrations.

Table 2
Intra-particle diffusion constants for the phosphorus adsorption onto HPA-Fe/C-B adsorbent.

Concentration (mg-P/L)	$t^{1/2}$ ($min^{1/2}$)	K_d (mg/(g·$min^{1/2}$))	C	R^2	r
2	0–4.5 (< 20 min)	8.04E-3	1.27E-1	0.9453	0.9793
		1.02E-3	1.72E-1	0.9518	0.9788
		5.52E-5	1.95E-1	0.9617	0.9871
5	4.5–26.8 (20–722 min)	2.58E-2	1.96E-1	0.9518	0.9838
		8.38E-3	2.81E-1	0.9862	0.9939
		5.35E-5	4.85E-1	0.9933	0.9983
10	26.8–53.7 (> 722 min)	7.51E-2	2.18E-1	0.9910	0.9970
		1.42E-2	4.63E-1	0.9971	0.9987
		1.71E-4	8.54E-1	0.9347	0.9835

Kinetic and equilibrium adsorption experiments provide information necessary for the design and operation of phosphate removal process in water/wastewater treatment. Different kinetic model may yield different parameter estimations [30]. In this study, four different classical kinetic models, namely, the pseudo-first-order (Fig.S1), the modified pseudo-first-order (Fig.S2), the pseudo-second-order (Fig.S3), the Elovich (Fig.S4), and the intra-particle diffusion model (Fig. 10), are used to fit the experimental data. Results show that the intra-particle diffusion model fits best the kinetic data.

According to the intra-particle diffusion model, a plot of q_t against $t^{1/2}$ should give a straight line with slope k_d and intercept C [31,32,2], that is (Eq. (6)):

$$q_t = K_d t^{1/2} + C \quad (6)$$

where K_d is the intra-particle diffusion rate constant, mg/(g $min^{1/2}$) and C is a constant. The C value is related to the thickness of adsorption boundary layer, therefore, the larger the C, the greater boundary layer effect. As seen in Table 2, the correlation coefficients, R^2 & r (Pearson correlation coefficient), for phosphorus adsorption onto the HPA-Fe/C-B is 0.9453–0.9971 & 0.9788–0.9987. The results show that the intra-particle diffusion kinetic model describes the experimental data well. Results (Table 2 & Fig. 10) show three distinct adsorption stages. The first stage is a rapid adsorption process occurring at $t^5 = 4.5\ min^{1/2}$ (or $t = 20$ min) in which phosphate adsorbs on the macropores surface readily. Adsorption on the mesopores surface takes place next at t^5 of 4.5–26.8 $min^{1/2}$ (or t = 20–722 min). Finally, adsorption proceeds to occupy the micropores surface at $t^5 > 26.8\ min^{1/2}$ (or $t >$ 722 min).

Table 2 gives k_d, C, R^2 and r of data fitting according to the intra-particle diffusion model. Table S1 summarizes the variables of kinetic models, i.e., k_1, k_2, a_e, b_e, and q_e at different initial phosphorus concentrations.

3.4. Adsorption isotherm

To optimize the design of an adsorption system for the adsorption of phosphorus from water/wastewater using HPA-Fe/C-B adsorbent, it is

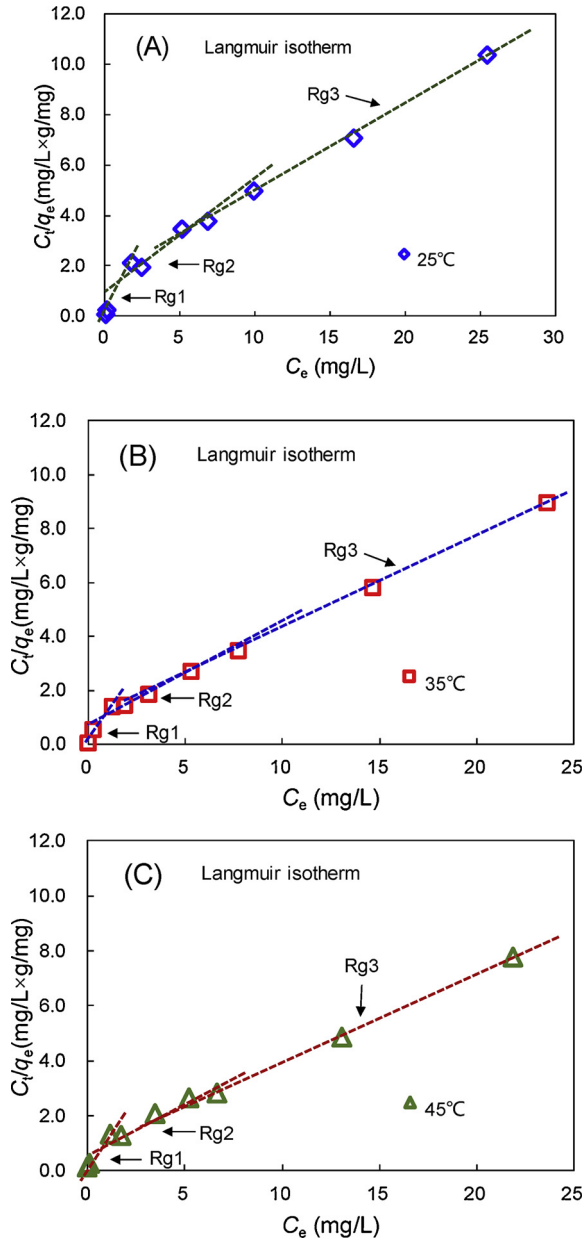

Fig. 11. Linearized Langmuir adsorption isotherm for phosphorus adsorption onto HPA-Fe/C-B at temperature 25 °C (a), 35 °C (b), and 45 °C (c), respectively. Where Rg standards for region. Experimental conditions: initial phosphorus concentration = 2, 5, & 10 mg/L; initial pH = 3.0; adsorbent dose = 10 g/L; geometric mean adsorbent grain size = 0.11 mm.

important to establish the most appropriate adsorption isotherm. In this study, the equilibrium adsorption data are fitted with Langmuir and Fruendlich adsorption isotherms at temperature 25, 35, and 45 °C, respectively (Fig.S5 and Table S2). Results show Langmuir adsorption isotherm has larger R^2 and r than that of the Fruendlich adsorption isotherm. The Langmuir adsorption isotherm has the following linearized equation (Eq. (7)):

$$C_e/q_e = 1/(q_m \cdot K_L) + C_e/q_m \quad (7)$$

where C_e is the equilibrium phosphorus concentration (mg/L), q_m is the monolayer adsorption capacity (mg/g), and K_L is the adsorption constant (L/mol). A plot of C_e/q_e versus C_e (Fig. 11) yields q_m and K_L from the slope and intercept of the linear plot (Table 3). The standard free energy (ΔG°, kJ/mol), enthalpy (ΔH°, kJ/mol) and entropy (ΔS°, kJ/(mol K)) of the adsorption process can be calculated from K_L and temperature by the following equation (Eq. (8)):

$$\Delta G^\circ = -RT\ln K_L = \Delta H^\circ - T\Delta S^\circ \quad (8)$$

where R is the gas constant 8.3145 J/mol-K (or 1.9863 cal/mol-K), K_L is the Langmuir adsorption constant (M^{-1}, L/mol).

Fig. 11 shows the linearized plot of Langmuir adsorption isotherm at 25, 35 and 45 °C, respectively. It is interesting to note that the adsorption isotherm is best fitted with the linearized Langmuir adsorption isotherm in three distinct regions with respect to equilibrium phosphorous concentrations, i.e., region 1 from 0 to 15 mg-P/L, region 2 from 15 to 30 mg-P/L, and region 3 from 30 to 50 mg-P/L. Conformation of the experimental data with Langmuir adsorption isotherm model with high R^2 & r value indicates the homogeneous nature of the adsorbent surface. Raising the temperature improves the adsorption capacity from 2.85 mg/g at 25 °C, to 2.89 mg/g at 35 °C, and to 3.08 mg/g at 45 °C. K_L value (in region 1, 2, and 3) indicates that the higher phosphorus concentration the larger adsorption energy.

The calculated ΔG° value is −29.9, −23.6, and −22.3 kJ/mol (or −7.1, −5.6, and −5.3 kcal/mol) for region 1 adsorption; −30.5, −24.0, and −23.7 kJ/mol (or −7.5, −5.9, and −5.8 kcal/mol) for region 2 adsorption, and −31.0, −24.3, and −23.9 kJ/mol (or −7.9, −6.2, and −6.1 kcal/mol) for region 3 adsorption at 25, 35 and 45 °C, respectively. Negative ΔG° value indicates spontaneous nature of adsorption. The ΔH° value calculated is −26.0, −20.6 and −18.4 kJ/mol *(or −6.2, −4.9, and −4.4 kcal/mol)* for the adsorption region 1, 2, and 3, respectively. The ΔS° value calculated is 158, 117, and 163 J/mol-K (or 37.8, 28.0 and 39.0 cal/mol-K) for the adsorption region 1, 2, and 3, respectively. Results of the thermodynamic analysis of equilibrium adsorption data are consistent with the kinetic aspects. Adsorption domain is consisted of three distinct regions, namely, Region 1, 2 and 3 with respect to filling the macropores, the mesopores, and the micropores, respectively. The change of enthalpy for all three regions are negative, meaning the exothermic nature of the adsorption process. The change of enthalpy (negative value) follows the order: $\Delta H_1 > \Delta H_2 > \Delta H_3$ and the change of entropy also follows the same order, ΔS_1–$\Delta S_3 > \Delta S_2$, respectively. Intuitively, less energy is involved

Table 3
Langmuir isotherm and thermodynamic parameters for phosphorus adsorption onto HPA-Fe/C-B.

T (°C)	q_m (mg-P/g)	K_L (M^{-1})	R_L	R^2	r	ΔG° (kJ/mol)	ΔH° (kJ/mol)	ΔS° (J/(mol·K)	ΔG° (kcal/mol)	ΔH° (kcal/mol)	ΔS° (cal/(mol·K
25	0.85	1.74E + 5	0.71E-2–3.47E-2	0.9982	0.9995	−29.9	−26.0	158	−7.2	−6.2	37.8
25	2.34	1.36E + 4	8.58E-2–1.35E-1	0.8871	0.9714	−23.6	−20.6	117	−5.6	−4.9	28.0
25	2.85	8.06E + 3	7.36E-2–1.17E-1	0.9964	0.9991	−22.3	−18.4	163	−5.3	−4.4	39.0
35	0.96	2.24E + 5	1.41E-2–6.67E-2	0.9453	0.9862	−30.5	−26.0	158	−7.2	−6.2	37.8
35	2.72	1.60E + 4	7.41E-2–1.18E-1	0.9961	0.9990	−24.0	−20.6	117	−5.7	−4.9	28.0
35	2.89	1.43E + 4	4.28E-2–6.93E-2	0.9996	0.9999	−23.7	−18.4	163	−5.7	−4.4	39.0
45	0.97	2.68E + 5	1.18E-2–5.63E-2	0.9991	0.9998	−31.0	−26.0	158	−7.4	−6.2	37.8
45	2.59	1.82E + 4	6.57E-2–1.05E-1	0.9737	0.9934	−24.3	−20.6	117	−5.8	−4.9	28.0
45	3.08	1.57E + 4	3.93E-2–6.38E-2	0.9994	0.9999	−23.9	−18.4	163	−5.7	−4.4	39.0

in phosphate ions adsorption onto the macropores and microspores. Greater entropy for phosphate ion adsorption onto the macroscpores and microposres indicate increase in the degree of organization of adsorbed anions, i.e., phosphate ions are more disorganized in microposres than in macropores.

A dimensionless parameter (R_L) that reflects the nature of adsorption is defined by the following equation (Eq. (9)):

$$R_L = 1/(1 + K_L C_o) \quad (9)$$

where K_L is the Langmuir adsorption constant and C_o is the initial phosphorus concentration (mg/L). R_L value reflects the trend of adsorption, i.e., unfavorable ($R_L > 1$), linear ($R_L = 1$), favourable ($0 < R_L < 1$) or irreversible ($R_L < 0$). Table 3 also shows R_L value to be near zero, which confirms favourable uptake of phosphorus [33].

4. Conclusions

The HPA-Fe/C-B adsorbent can effectively remove phosphorus from aqueous solution. The phosphorus adsorption capacity of the pulverized HPA-Fe/C-B adsorbent ($d_g = 0.11$ mm) at 25 °C and pH 3, reaches equilibrium at 60, 720, and 1080 min and initial phosphorus concentration of 2, 5, and 10 mg/L, respectively. The phosphorus adsorption capacity increases from 0.20 to 2.46 mg/g, to 2.62 mg/g, and then to 2.81 mg/g at 25 °C, 35 °C, and 45 °C, respectively, in the initial phosphorus concentration range of 2–50 mg/L. The optimal adsorption pH is 3.0. The maximal phosphorus removal is 99.2, 97.5, and 84.4%, at the initial phosphorus concentration of 2, 5, and 10 mg/L, respectively. The adsorption capacity of unpulverized HPA-Fe/C-B adsorbent ($d_g = 1.59$ mm) is 0.18, 0.36, and 0.66 mg/g, at initial phosphorus concentration of 2, 5, and 10 mg/L, respectively. The phosphorus adsorption capacity of HPA-Fe/C-B is greater than nano- and micro-sized of iron oxides particles reported in the literature.

Multiple-stage, intra-particle diffusion model describes the kinetics of phosphate adsorption onto HPA-Fe/C-B adsorbent well. At initial phosphorus concentration of 2, 5, and 10 mg/L, the correlation coefficients, R^2 & r for kinetic adsorption data fitting is in the range of 0.9453–0.9971 & 0.9788–0.9987 for the three adsorption regions. Langmuir adsorption isotherm fits better than the Fruendlich adsorption isotherm in three distinct regions with respect to initial phosphorus concentration. The R_L value is between 0.0071 and 0.1176, which indicate favourable adsorption. The negative ΔG° value implies spontaneous nature of adsorption over the temperature range studied.

Acknowledgements

Authors greatly appreciate the insightful comments of our anonymous reviewers. The authors wish to thank the Guangxi Key Laboratory of Environmental Pollution Control Theory and Technology for the research assistance and the financial supports from the National Natural Science Foundation of China (NSFC21707024, NSFC41763012) and the US, National Science Foundation (EPSCoR 1632899).

Appendix A. Supplementary data

Supplementary data associated with this article can be found, in the online version, at https://doi.org/10.1016/j.jwpe.2018.05.010.

References

[1] C.P. Huang, Removal of phosphate by powdered aluminium oxide adsorption, J.-Water Pollut. Control Fed. 8 (1977) 1811–1817.
[2] S. Sawayama, K.K. Rao, D.O. Hall, Nitrate and phosphate ion removal from water by phormidium laminosum immobilized on hollow fibres in a photobioreactor, Appl. Microbiol. Biot. 49 (1998) 463–468.
[3] S.Y. Yoon, C.G. Lee, J.A. Park, J.H. Kim, S.B. Kim, S.H. Lee, J.W. Choi, Kinetic, equilibrium and thermodynamic studies for phosphate adsorption to magnetic iron oxide nanoparticles, Chem. Eng. J. 236 (2014) 342–347.
[4] M. Rashid, N.T. Price, M.A.G. Pinilla, K.E. O'Shea, Effective removal of phosphate from aqueous solution using humic acid coated magnetite nanoparticles, Water Res. 123 (2017) 353–360.
[5] G.S. Zhang, H.J. Liu, R.P. Liu, J.H. Qu, Removal of phosphate from water by a Fe-Mn binary oxide adsorbent, J. Colloid Interface Sci. 335 (2009) 168–174.
[6] N. Liu, A.B. Charrua, C.H. Weng, X.L. Yuan, F. Ding, Characterization of biochars derived from agriculture wastes and their adsorptive removal of atrazine from aqueous solution: a comparative study, Bioresour. Technol. 198 (2015) 55–62.
[7] C.P. Huang, Adsorption of phosphate at the hydrous γ-Al_2O_3?electrolyte interface, J. Colloid Interface Sci. 53 (2) (1975) 178–186.
[8] P. Loganathan, S. Vigneswaran, J. Kandasamy, Removal andREcovery of phosphate from water usng sorption, Crit. Rev. Environ. Sci. Technol. 44 (2014) 847–907.
[9] A. Dremkova-Tuhtah, K. Mandel, A. Paulus, C. Meyer, F. Hunter, C. Gellermann, G. Sextl, M. Fanzreb, H. Steinmetz, Phosphate recovery from wastewater using engineered superparamagnetic particles modified with layered double hydroxide ion exchangers, Water Res. 47 (2013) 5670–5677.
[10] K. Mandel, A. Drenkova, F. Hunter, C. Gellermann, H. Steinmetz, G. Sextl, Layered double hydroxide ion exchangers on superparamagnetic microparticles for recovery of phosphate from wastewater, J. Mater. Chem.A 1 (2013) 1840–1848.
[11] L.G. Yan, K. Yang, R.R. Shan, T. Yan, J. Wei, S.J. Yu, H.Q. Yu, B. Du, Kinetic, isotherm and thermodynamic investigations of phosphate adsorption onto core-shell Fe_3O_4@LDHs composites with easy mangetic separation assistance, J. Colloid Interfce Sci. 448 (2015) 508–516.
[12] L.P. Fang, B. Wu, I.M.C. Lo, Fabrication of silica-free superparamagnetic ZrO_2@Fe_3O_4 with enhanced phosphate recovery from sewage: performance and adsorption mechanism, Chem. Eng. J. 319 (2017) 258–267.
[13] Z.Q. Zhu, Y.N. Zhu, H. Qin, Y.H. Li, Y.P. Liang, H. Deng, H.L. Li, Preparation and properties of porous composite of Hematite/Magnetite/Carbon with eucalyptus wood biotemplate, Mater. Manuf. Processes 3 (2015) 285–291.
[14] X.L. Qu, P.J.J. Alvarez, Q.L. Li, Applications of nanotechnology in water and wastewater treatment, Water Res. 12 (2013) 3931–3946.
[15] Y.H. Li, Y.N. Zhu, Z.Q. Zhu, W.H. Wei, H. Deng, Y.P. Liang, X.H. Zhang, D.Q. Wang, Kinetics and thermodynamics of adsorption for arsenate ions on the hierarchical porous adsorbent of α-Fe_2O_3/Fe_3O_4/C with bamboo bio-template, Desalin. Water Treat. 76 (2017) 276–289.
[16] Z.Q. Zhu, H.H. Zeng, Y.N. Zhu, F. Yang, H.X. Zhu, H. Qin, W.H. Wei, Kinetics and thermodynamic study of phosphate adsorption on the porous biomorph-genetic composite of a-Fe_2O_3/Fe_3O_4/C with eucalyptus wood microstructure, Sep. Puref. Technol. 117 (2013) 124–130.
[17] Q. Liu, H. Pan, J. Wang, L.J. Zhang, R.H. Huang, Phosphate adsorption from aqueous solutions by Zirconium(IV) loaded cross-linked chitosan particles, J. Taiwan Inst. Chem. Eng. 59 (2016) 311–319.
[18] R.M. Cornell, U. Schwertmann, The Iron Oxides: Structure, Properties, Reactions, Occurrences, and Uses, second ed., Wiley-VCH, Weinheim, 2003.
[19] G. Muñiz, V. Fierro, A. Celzard, G. Furdin, G. Gonzalez-Sánchez, M.L. Ballinas, Synthesis, characterization and performance in arsenic removal of iron-doped activated carbons prepared by impregnation with Fe(III) and Fe(II), J. Hazard. Mater. 165 (2009) 893–902.
[20] C.H. Weng, C.P. Huang, H.E. Allen, P.F. Sanders, Cr(VI) adsorption onto hydrous concrete particles from groundwater, J. Environ. Eng. 12 (2001) 1124–1131.
[21] T.M. Barber, Phosphate Adsorption by Mixed and Reduced Iron Phases, Master Degree Thesis, Stanford University, U.S, 2018http://soils.stanford.edu/theses/Theresa_Barber.pdf.
[22] J. Choi, J. Chung, W. Lee, J.O. Kim, Phosphorous adsorption on synthesized magnetite in wastewater, J. Ind. Eng. Chem. 34 (2016) 198–203.
[23] C. Colombo, V. Barron, J. Torrent, Phosphate adsorption and desorption in relation to morphology and crystal properties of synthetic hematites, Geochim. Cosmochim. Acta 58 (1994) 1261–1269.
[24] S. Kuo, E.G. Lotse, Kinetics of phosphate adsorption and desorption by hematite and gibbsite, Soil Sci. 6 (1974) 400–406.
[25] A. Dimirkou, A. Ioannou, M. Doula, Preparation, characterization and sorption properties for phosphates of hematite, bentonite and bentonite-hematite systems, Adv. Colloid Interface 97 (2002) 37–60.
[26] A. Ioannoua, A. Dimirkou, Phosphate adsorption on hematite, kaolinite, and kaolinite–hematite (k-h) systems as described by a constant capacitance model, J. Colloid. Interface Sci. 192 (1997) 119–128.
[27] T.J. Daou, S. Begin-Colin, J.M. Grene'che, F. Thomas, A. Derory, P. Bernhardt, P. Legaré, G. Pourroy, Phosphate adsorption properties of magnetite-Based nanoparticles, Chem. Mater. 19 (2007) 4494–4505.
[28] G. Pan, L. Li, D.Y. Zhao, H. Chen, Immobilization of non-point phosphorus using stabilized magnetite nanoparticles with enhanced transportability and reactivity in soils, Environ. Pollut. 158 (2010) 35–40.
[29] X. Huang, Intersection of isotherms for phosphate adsorption on hematite, J. Colloid. Interface Sci. 271 (2004) 296–307.
[30] Y. Akio, Diverse secondary interactions between ions exchanged into the resin phase and their analytical application, Ansl. Sci. 30 (2014) 51–57.
[31] C.H. Weng, C.Z. Tsai, S.H. Chua, Y.C. Sharma, Adsorption characteristics of copper (II) onto spent activated clay, Sep. Purif. Technol. 54 (2007) 187–197.
[32] W.J. Weber, J.C. Morris, Kinetics of adsorption on carbon from solution, J. Sanit. Eng. Div. Am. Soc. Civ. Eng. 89 (1963) 31–60.
[33] G. Mckay, V.J.P. Poots, Kinetics and diffusion process in colour removal from effluent using wood as an adsorbent, J. Chem. Technol. Biotechnol. 30 (1980) 279–292.